

# Reconstruction of laser beam wavefronts based on mode analysis

Christian Schulze,<sup>1,\*</sup> Angela Dudley,<sup>2</sup> Daniel Flamm,<sup>1</sup>  
Michael Duparré,<sup>1</sup> and Andrew Forbes<sup>2</sup>

<sup>1</sup>Institute of Applied Optics, Abbe Center of Photonics, Friedrich Schiller University, Fröbelstieg 1, 07743 Jena, Germany

<sup>2</sup>Council for Scientific and Industrial Research, National Laser Centre, P.O. Box 395, 0001 Pretoria, South Africa

\*Corresponding author: christian.schulze@uni-jena.de

Received 17 May 2013; revised 26 June 2013; accepted 26 June 2013;  
posted 27 June 2013 (Doc. ID 190739); published 19 July 2013

We present the reconstruction of a laser beam wavefront from its mode spectrum and investigate in detail the impact of distinct aberrations on the mode composition. The measurement principle is presented on a Gaussian beam that is intentionally distorted by displaying defined aberrations on a spatial light modulator. The comparison of reconstructed and programmed wavefront aberrations yields excellent agreement, proving the high measurement fidelity. © 2013 Optical Society of America

*OCIS codes:* (140.3295) Laser beam characterization; (010.7350) Wave-front sensing; (120.5050) Phase measurement; (030.4070) Modes; (070.6120) Spatial light modulators.  
<http://dx.doi.org/10.1364/AO.52.005312>

## 1. Introduction

Naturally, every laser beam gathers a certain amount of aberration during its propagation. Possible reasons are imperfect optical elements or the inhomogeneity of the propagation medium itself, usually the atmosphere. Corresponding studies of inhomogeneous and turbulent media [1,2] have been considered significant in application fields such as terrestrial observation [3] and communication [4], but also in fields like microscopy [5] and ophthalmology [6], which require high-resolution imaging and rely on precise wavefront estimation. By means of adaptive optics the measured wavefronts are corrected, which yields an enhanced beam quality and therefore, e.g., an improved spatial resolution. Such closed-loop approaches have not only been reported in astronomy and microscopy but also found application in micromanipulation [7]. In terms of free space communication, beams carrying orbital angular momentum and the impact of atmospheric-turbulence-induced aberrations on their

propagation are of particular interest [8,9]. Different wavefront measurement techniques exist, including ray tracing [10], pyramid sensors [11], interferometric approaches [12,13], the widely used Shack–Hartmann sensor [14], nonlinear approaches for high-intensity light pulses [15], the application of multiplexed holograms to detect a set of selected Zernike modes [16], and the use of correlation filters [17].

In this work we demonstrate the reconstruction of a laser beam wavefront from its mode spectrum and systematically investigate the influence of defined wavefront distortions on the modal composition of the beam. As will be shown, each aberration yields a characteristic distortion of the mode spectrum similar to a fingerprint. The modal decomposition of the beam is performed using correlation filters, which enable a wavefront reconstruction that stands out from other techniques due to its high spatial resolution, increased measurement area, and large measurable wavefront slope, while maintaining the capability for real-time measurements. As a vivid example we distorted a Gaussian beam with various Zernike aberrations that are programmed on a spatial light modulator (SLM) successively and demonstrated

the impact on the mode spectrum. The excellent agreement of measured and programmed aberrations indicates the reliability and high fidelity with which the wavefront can be reconstructed and emphasizes the relevance of the technique as a diagnostic tool in the fields of microscopy, micro-manipulation, and free space communication.

The paper is organized as follows. Section 2 outlines the basics of the modal decomposition and its application to reconstruction of the wavefront, Section 3 demonstrates the impact of aberrations on the modal power spectrum, and Sections 4 and 5 present the experimental setup and the measurement results, followed by the conclusion in Section 6.

## 2. Wavefront Reconstruction by Modal Decomposition

Every monochromatic laser field  $U \exp(i\omega t)$  with angular frequency  $\omega$  can be considered as the superposition of a number of transverse modes. Consider, for example, the decomposition into a set of Laguerre–Gaussian modes of free space (time dependence omitted):

$$U(\mathbf{r}) = \sum_{p,l} \rho_{p,l} u_{p,l}(\mathbf{r}) \exp(i\phi_{p,l}), \quad (1)$$

where  $\mathbf{r} = (x, y)$  denotes the spatial coordinates,  $u_{p,l}$  is the Laguerre–Gaussian mode with radial index  $p$  and azimuthal index  $l$  at its waist position ( $z = 0$ ) [18], and  $\rho_{p,l}^2$  and  $\phi_{p,l}$  are its power and phase (relative to a reference mode), respectively. Finding the modal powers  $\rho_{p,l}$  and phases  $\phi_{p,l}$  from a given set of orthogonal modes is the purpose of the modal decomposition approach [19]. The knowledge about the above parameters enables one to recover the optical field in amplitude and phase, and finally to reconstruct the wavefront  $W$  by minimizing the integral [20]:

$$\iint |\mathbf{P}| \left| \frac{\mathbf{P}_t}{|\mathbf{P}|} - \nabla_t W \right|^2 dA \rightarrow \min, \quad (2)$$

where  $t$  marks transverse components,  $\nabla_t = [\partial x, \partial y]$ ,  $dA$  is the surface element, and  $\mathbf{P}$  is the Poynting vector distribution of the beam.  $\mathbf{P}$  is directly related to the optical field  $U$  [17]:

$$\mathbf{P}(\mathbf{r}) = \frac{\varepsilon_0 \omega}{4} [i(U \nabla_t U^* - U^* \nabla_t U) + 2k|U|^2 \mathbf{e}_z], \quad (3)$$

where  $\omega$  is the angular frequency,  $\varepsilon$  is the permittivity,  $\varepsilon_0$  is the permittivity of vacuum,  $k = 2\pi/\lambda$  is the wave number, and  $\mathbf{e}_z$  is the unit vector in  $z$  direction.

The reconstruction of the optical field (and consequently of the Poynting vector distribution and wavefront) is done using the correlation filter technique [19], the core details of which we outline here for the benefit of the reader. Accordingly, a computer-generated hologram that acts as a matched filter correlates the laser beam under investigation with a given mode set. The result of such an inner product

measurement then appears as an intensity value  $I = \iint T^*(\mathbf{r})U(\mathbf{r})d^2\mathbf{r}$  on the optical axis in the Fourier plane of the hologram, where  $T$  denotes the transmission function of the hologram, and “\*” marks complex conjugation [21]. The hologram transmission function necessary to measure the power content of one mode takes the form

$$T_{p,l}(\mathbf{r}) = u_{p,l}^*(\mathbf{r}). \quad (4)$$

Using this transmission function, the correlation signal behind the hologram appears to be  $I_{p,l}^\rho \propto \rho_{p,l}^2$ , where the modal powers  $\rho_{p,l}^2$  are normalized to unit power by  $\sum_{p,l} \rho_{p,l}^2 = 1$ . To also measure the relative phases of the modes  $u_{p,l}$  to a chosen reference field  $u_{\text{ref}}$ , the transmission function is changed to contain a phase-dependent superposition of mode and reference field:

$$\begin{aligned} T_{p,l}^{\cos}(\mathbf{r}) &= [u_{\text{ref}}^*(\mathbf{r}) + u_{p,l}^*(\mathbf{r})]/\sqrt{2}, \\ T_{p,l}^{\sin}(\mathbf{r}) &= [u_{\text{ref}}^*(\mathbf{r}) + iu_{p,l}^*(\mathbf{r})]/\sqrt{2}. \end{aligned} \quad (5)$$

Using such transmission functions, the far-field intensity on the optical axis becomes dependent on the relative phase  $\phi_{p,l}$  to the reference field with power  $\rho_{\text{ref}}^2$ :

$$\begin{aligned} I_{p,l}^{\sin} &\propto \rho_{\text{ref}}^2 + \rho_{p,l}^2 + 2\rho_{\text{ref}}\rho_{p,l} \sin \phi_{p,l}, \\ I_{p,l}^{\cos} &\propto \rho_{\text{ref}}^2 + \rho_{p,l}^2 + 2\rho_{\text{ref}}\rho_{p,l} \cos \phi_{p,l}. \end{aligned} \quad (6)$$

Accordingly, the relative phase  $\phi_{p,l}$  can be calculated by

$$\phi_{p,l} = -\arctan \left[ \frac{2I_{p,l}^{\sin} - I_{p,l}^\rho - I_{\text{ref}}^\rho}{2I_{p,l}^{\cos} - I_{p,l}^\rho - I_{\text{ref}}^\rho} \right], \quad (7)$$

where  $I_{p,l}^{\sin}$  and  $I_{p,l}^{\cos}$  depict the intensity signals from the inner product (phase) measurements. Thereby, the reference field in Eq. (5) is arbitrary but should be a mode that is contained in the beam with a reasonable amount of power (>5% of total power) to yield meaningful results for the phase measurement. Physically, correlation filters can be implemented using phase-only SLMs [22] or solid amplitude-only filters [19] by employing special coding techniques to transfer the complex-valued transmission function to a phase-only [23] or an amplitude-only function [24], respectively. When all the modal powers and phases are measured, the optical field, Poynting vector, and wavefront can be reconstructed according to Eqs. (1)–(3).

## 3. Distortion of the Modal Spectrum

For the aberration we consider a phase distortion to the initial field  $U_i$  of the kind

$$U = U_i \exp(i\pi b Z_{nm}), \quad (8)$$

where  $Z_{nm}$  is the Zernike polynomial of radial order  $n$  and azimuthal order  $m$  [25], and  $b$  is the aberration strength in the form of a simple weighting factor. Since Laguerre–Gaussian modes represent a complete set in free space and follow the same azimuthal symmetry as the Zernike polynomials, they are an appropriate choice as basis set for decomposition. Consider, for example, the distortion of a fundamental Gaussian beam by the aberration of defocus and its decomposition into the set of Laguerre–Gaussian modes, as seen in Fig. 1. The decomposition of the unaberrated beam [Figs. 1(a) and 1(b), no wavefront curvature added] yields a simple mode spectrum with 100% fundamental mode content. However, when such a beam [Fig. 1(d)] is aberrated with defocus [Fig. 1(e)], its modal spectrum becomes distorted, which means that modes other than the fundamental one appear, yielding a fundamental mode power  $\rho_{0,0}^2 < 1$  [Fig. 1(f)]. Thus, each aberration not only distorts the wavefront or far-field intensity, but it also influences the modal power spectrum  $\rho_{p,l}^2$  and phase spectrum  $\phi_{p,l}$ , which means that additional modes appear that solely result from the aberration. Moreover, the fundamental mode content  $\rho_{0,0}^2 \leq 1$  can be considered here as a quantity very similar to the Strehl ratio [25], which is often used in optical turbulence and adaptive optics, and which also simplifies the impact of aberrations into one scalar number by comparing the perturbed and unperturbed on-axis intensity values.

Figure 2 depicts the expected fundamental mode response as a function of the strength  $b$  of different Zernike aberrations. As expected, with increasing aberration strength, the relative fundamental mode content decreases from 1 to 0, but with different slopes for the specific aberrations. Apparently, coma ( $Z_{31}$ ) and spherical aberration of third order ( $Z_{40}$ ) yield the fastest drop in fundamental mode content, whereas increasing the strength of trefoil ( $Z_{33}$ ) only leads to a gradual decrease. The reason for this dependence is simply found in the different shapes of the aberrations. While all Zernike aberrations are normalized to unit power within a defined radius (which was chosen to be the same for all aberrations in Fig. 2), the overlap with a fundamental Gaussian

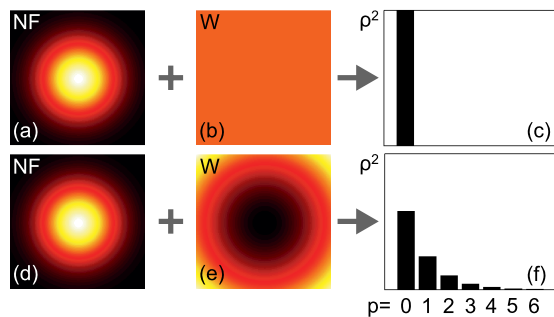


Fig. 1. Decomposition (a)–(c) of an ideal fundamental Gaussian beam and (d)–(f) of the same beam aberrated with defocus. NF, near field intensity; W, wavefront;  $\rho^2$ , modal power spectrum.

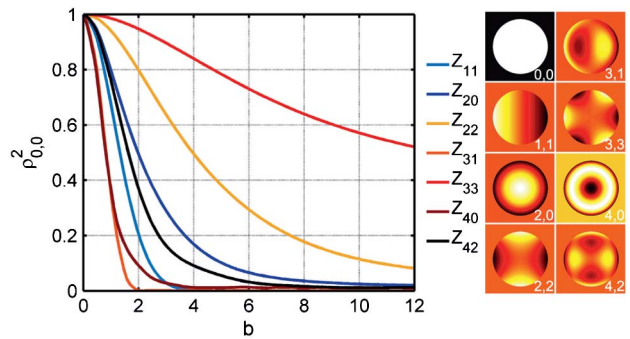


Fig. 2. Simulated relative fundamental mode content  $\rho_{0,0}^2$  as a function of aberration strength  $b$ . Insets depict the shapes of the corresponding aberrations.

mode differs, yielding a stronger impact of those aberrations that have a greater overlap.

#### 4. Experimental Setup

To measure the influence of defined Zernike aberrations on a laser beam, we used an experimental setup as outlined in Fig. 3. The beam of a helium–neon laser (10 mW power, 633 nm wavelength) was expanded and collimated [ $f(L_1) = 15$  mm,  $f(L_2) = 125$  mm] to approximate a plane wave when illuminating the first SLM (SLM<sub>1</sub>, Pluto Holoeye, 1920 × 1080 pixels, 8 μm pixel pitch, reflective). Using complex amplitude modulation [23], we generated a fundamental Gaussian beam (waist radius  $w_0 = 0.25$  mm) and superimposed it with the aberrations stated in Fig. 2. Therefore, the definition radius of the Zernike aberrations (Zernike radius) was chosen to be  $2.5 \times w_0$  to avoid deterioration of the beam intensity in the near field, which potentially occurs due to the limited definition region of the Zernike polynomials. The aberration strengths were chosen such that all aberrations yielded a comparable impact on the beam, e.g., in terms of decrease in fundamental mode content. The plane of SLM<sub>1</sub> was relay imaged [ $4f$ -imaged,  $f(L_3) = f(L_4) = 500$  mm] onto a second SLM (SLM<sub>2</sub>, same specifications as SLM<sub>1</sub>), which was used to perform the modal decomposition of the aberrated beam. An aperture placed in the Fourier plane of SLM<sub>1</sub> acted as a filter to separate the desired (first diffraction order) from the undiffracted light (zeroth diffraction order). A camera was placed in the Fourier plane [ $f(L_5) = 300$  mm] of SLM<sub>2</sub>, enabling us to detect

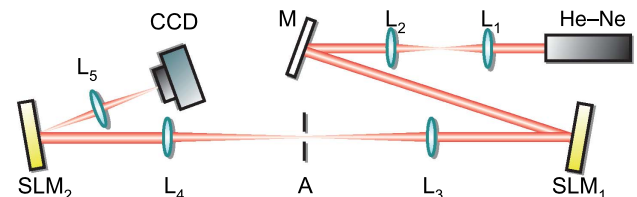


Fig. 3. Schematic of the experimental setup to modally decompose differently aberrated Gaussian beams. He–Ne, helium–neon laser;  $L_{1-5}$ , lenses; M, mirror; SLM<sub>1,2</sub>, spatial light modulator (actually reflective); A, aperture; CCD, camera.

the modal power and phase spectrum by recording the intensities  $I_{p,l}^p$ ,  $I_{p,l}^{\sin}$ , and  $I_{p,l}^{\cos}$  when displaying the transmission functions  $T_{p,l}^p$ ,  $T_{p,l}^{\sin}$ , and  $T_{p,l}^{\cos}$ . Since the SLM can be dynamically addressed, we displayed all of the transmission functions sequentially, one after the another. Accordingly, the temporal measurement effort was in the range of a few seconds but can be increased to real time by using multiplexed holograms [19]. For the reference field we chose the fundamental mode  $u_{\text{ref}} = u_{0,0}$ , since it is expected to keep the highest mode content in the range of investigated aberration strengths.

## 5. Results

To test the wavefront reconstruction procedure described in Section 2, we generated a fundamental Gaussian beam, distorted it with Zernike aberrations of different orders, and decomposed the aberrated beams into the set of Laguerre–Gaussian modes. Therefore, every aberration leads to a characteristic distortion of the mode spectrum. As an example, Fig. 4 depicts the decomposition results for an aberration of tilt. The chosen aberration strength of  $b = 1$  yields a drop in fundamental mode power to 55%, as shown in Fig. 4(a), and consequently a dispersion of the power to other modes, especially to modes of neighboring  $l$  values:  $u_{p,\pm 1}$  (18%). Small mode power is also dispersed among modes of higher  $l$  value ( $|l| > 2$ ) and higher  $p$  value ( $p > 0$ ) with powers  $< 3\%$ . Whereas the shape of the mode spectrum is characteristic for the kind of aberration, the exact mode power levels depend on the chosen aberration strength, e.g., the fundamental mode content strongly decreases with increasing strength (Fig. 2). The wavefront distortion affects not only the modal power spectrum but also the spectrum of relative phases as shown in Fig. 4(b). The exact phase shift between the different higher order modes is necessary to reconstruct the wavefront

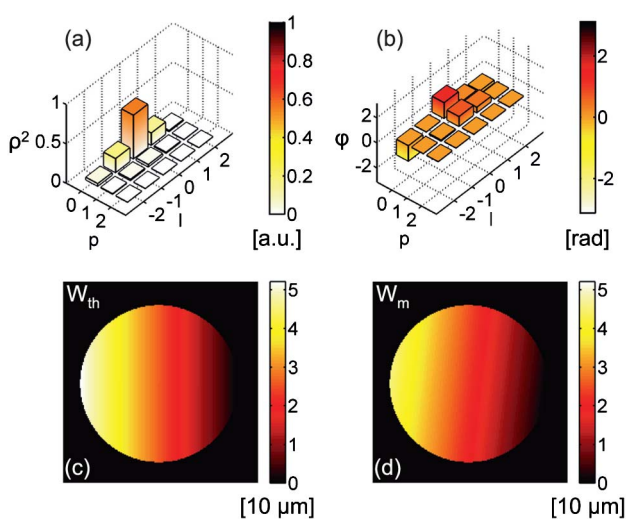


Fig. 4. Modal decomposition of a Gaussian beam aberrated with tilt. (a) Modal power spectrum, (b) modal phase spectrum, (c) theoretically expected wavefront, and (d) measured wavefront.

aberration correctly. Figures 4(c) and 4(d) show the theoretically expected and measured (reconstructed) wavefront in units of  $10 \mu\text{m}$ . It can be seen that both wavefronts are in excellent agreement regarding shape and absolute scale. A more quantitative comparison is achieved using the two-dimensional cross-correlation coefficient [26], which ranges between 0 (no correlation) and 1 (complete correlation), yielding a value of 0.99 for tilt. The spatial resolution of the reconstructed wavefront is  $200 \times 200$  pixels in the depicted range. However, this value can be increased significantly and is only dependent on the resolution with which the modes for decomposition can be calculated.

A second example is given in Fig. 5. Here, astigmatism ( $Z_{22}$ ) was induced by SLM<sub>1</sub> with an aberration strength of  $b = 3$ . From Fig. 5(a) it is evident that this yields a degradation in the fundamental mode content to 58%, which is similar to the previous case of tilt. Due to the normalization of the Zernike aberrations to unit power within the Zernike radius and the subsequently smaller overlap with the Gaussian, a higher aberration strength is needed in comparison to tilt to yield a similar effect on the mode spectrum. As is visible in Fig. 5(a), the spectrum is similar to the tilt spectrum, but since the azimuthal index of astigmatism  $m$  is 2, and only modes of  $|l| = N \times m$  occur ( $N = 0, 1, 2, \dots, p \geq 0$ , similar to higher harmonics), there are gaps in the spectrum, where  $|l|$  is odd. The exclusive response of modes with  $|l| = N \times m$  is reasonable, since both Laguerre–Gaussian modes and Zernike polynomials obey the same azimuthal dependence. Including the phase spectrum [Fig. 5(b)], the wavefront was reconstructed [Fig. 5(d)], agreeing well with the theoretically expected wavefront (correlation 0.99) depicted in Fig. 5(c). From the previous examples it becomes evident that only multiples of the aberration's azimuthal index appear in the mode

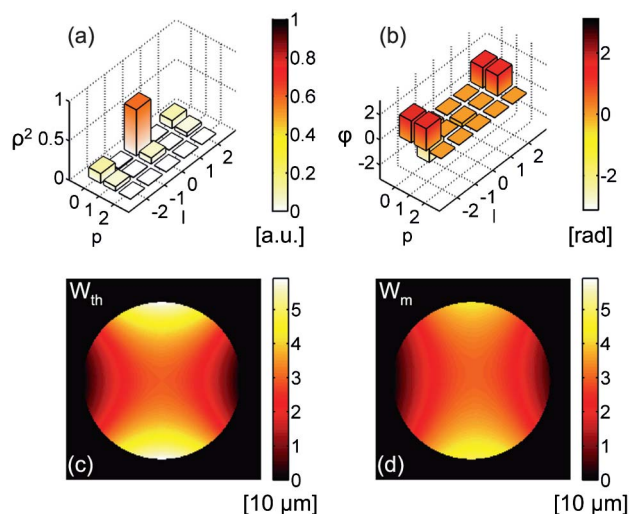


Fig. 5. Modal decomposition of a Gaussian beam aberrated with astigmatism. (a) Modal power spectrum, (b) modal phase spectrum, (c) theoretically expected wavefront, and (d) measured wavefront.

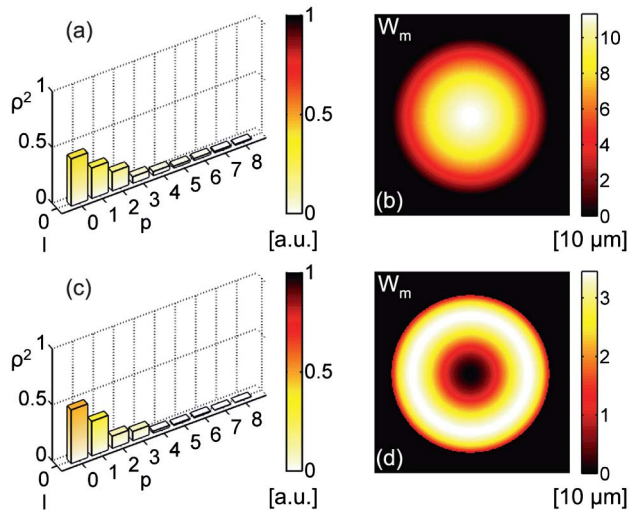


Fig. 6. Modal decomposition of a Gaussian beam aberrated with (a), (b) defocus and (c), (d) third order spherical. (a) Modal power spectrum, (b) reconstructed wavefront, (c) modal power spectrum, and (d) reconstructed wavefront.

spectra as  $l$  values of the modes. Accordingly, for radially symmetric aberrations where the azimuthal index  $m = 0$ , only modes of  $u_{p,0}$  are expected. Figure 6 depicts the results for the two aberrations of defocus ( $Z_{20}$ ) and spherical aberration of the third order ( $Z_{40}$ ), where we chose aberration strengths of  $b = 2$  and  $b = 1$ , respectively, to yield a similar impact on the mode spectrum. For both cases, the modal spectra [Figs. 6(a) and 6(c)] reveal a decay toward higher order modes with  $p \geq 0$  and  $l = 0$ . The measured wavefronts are shown in Figs. 6(b) and 6(d), revealing the typical shape for these kinds of aberrations.

The comparison of all measured wavefront aberrations with the theoretically expected deformations are summarized in Table 1, employing the two-dimensional correlation coefficient, revealing very good agreement for all investigated aberrations. The impact of each individual aberration can be observed from the different aberration strengths  $b$  necessary to yield a reduction in fundamental mode content to a percentage value  $\rho_{0,0}^2$ .

As an additional, independent proof that the SLM produced the aberrations as intended, we placed the camera in the Fourier plane (far field) of the first SLM (Fig. 7), where the aberrations become evident

Table 1. Summary of Results, Stating Aberration Strength  $b$ , Corresponding Relative Fundamental Mode Power  $\rho_{0,0}^2$ , and the Correlation Coefficient between the Theoretically Expected and Measured Wavefronts (Zernike Polynomials  $Z_{nm}$ )

$n$ (radial)	$m$ (azimuthal)	$b$	$\rho_{0,0}^2$ (%)	$C(W_{th}, W_m)$
1	1	1	55.4	0.99
2	0	2	42.1	0.99
2	2	3	58.4	0.99
3	1	0.8	51.0	0.87
3	3	12	59.4	0.92
4	0	1	47.7	0.99
4	2	1.5	54.8	0.97

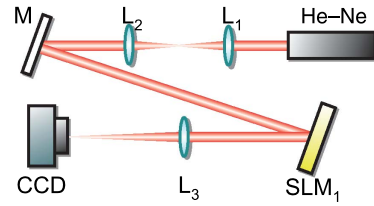


Fig. 7. Experimental setup for measuring the far field of differently aberrated Gaussian beams. He-Ne, helium-neon laser;  $L_{1-3}$ , lenses; M, mirror;  $SLM_1$ , spatial light modulator; CCD, camera.

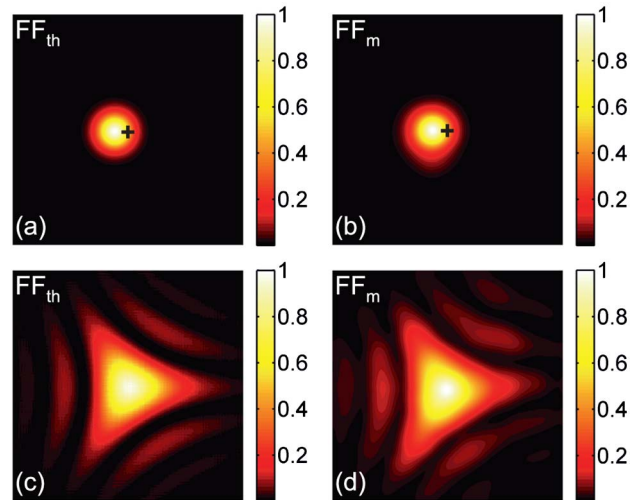


Fig. 8. Theoretical and measured far fields  $FF_{th}$  and  $FF_m$  of a fundamental Gaussian beam aberrated with (a), (b) tilt and (c), (d) trefoil.

also in the intensity distribution. Two examples are shown in Fig. 8, depicting the impact of tilt and trefoil on the far-field intensity. As expected, the fundamental Gaussian beam is merely shifted in the case of tilt, as indicated by a black cross (optical axis) in Figs. 8(a) and 8(b), depicting the theoretical and measured far field. When programming trefoil on  $SLM_1$ , the far-field intensity is strongly distorted, taking on a triangular shape. Again, the theoretical [Fig. 8(c)] and measured [Fig. 8(d)] far fields are in excellent agreement.

## 6. Conclusion

In conclusion, we presented a detailed investigation of the impact of different wavefront aberrations (Zernike aberrations) on the mode spectrum of a laser beam. We could show that each aberration leads to a very characteristic distortion of the modal power and phase spectrum, similar to a fingerprint. The knowledge about the mode powers and relative phases was used to reconstruct the wavefront of the beam quickly, in high spatial resolution, and with measurement fidelities reaching 99%. Accordingly, we consider our approach to be a versatile tool for wavefront diagnostics in numerous applications, such as microscopy, micromanipulation, and free space communication.

## References

1. L. W. Casperson, "Gaussian light beams in inhomogeneous media," *Appl. Opt.* **12**, 2434–2441 (1973).
2. R. F. Lutomirski and H. T. Yura, "Propagation of a finite optical beam in an inhomogeneous medium," *Appl. Opt.* **10**, 1652–1658 (1971).
3. F. Roddier, M. Séchaud, G. Rousset, P.-Y. Madec, M. Northcott, J.-L. Beuzit, F. Rigaut, J. Beckers, D. Sandler, P. Léna, and O. Lai, *Adaptive Optics in Astronomy* (Cambridge University, 1999).
4. J. C. Ricklin and F. M. Davidson, "Atmospheric turbulence effects on a partially coherent Gaussian beam: implications for free-space laser communication," *J. Opt. Soc. Am. A* **19**, 1794–1802 (2002).
5. M. A. A. Neil, R. Juakaitis, M. J. Booth, T. Wilson, T. Tanaka, and S. Kawata, "Adaptive aberration correction in a two-photon microscope," *J. Microsc.* **200**, 105–108 (2000).
6. B. Hermann, E. J. Fernández, A. Unterhuber, H. Sattmann, A. F. Fercher, W. Drexler, P. M. Prieto, and P. Artal, "Adaptive-optics ultrahigh-resolution optical coherence tomography," *Opt. Lett.* **29**, 2142–2144 (2004).
7. T. Cizmar, M. Mazilu, and K. Dholakia, "In situ wavefront correction and its application to micromanipulation," *Nat. Photonics* **4**, 388–394 (2010).
8. L. Marrucci, C. Manzo, and D. Paparo, "Optical spin-to-orbital angular momentum conversion in inhomogeneous anisotropic media," *Phys. Rev. Lett.* **96**, 163905 (2006).
9. G. Gbur and R. K. Tyson, "Vortex beam propagation through atmospheric turbulence and topological charge conservation," *J. Opt. Soc. Am. A* **25**, 225–230 (2008).
10. R. Navarro and E. Moreno-Barriuso, "Laser ray-tracing method for optical testing," *Opt. Lett.* **24**, 951–953 (1999).
11. S. R. Chamot, C. Dainty, and S. Esposito, "Adaptive optics for ophthalmic applications using a pyramid wavefront sensor," *Opt. Express* **14**, 518–526 (2006).
12. M. P. Rimmer and J. C. Wyant, "Evaluation of large aberrations using a lateral-shear interferometer having variable shear," *Appl. Opt.* **14**, 142–150 (1975).
13. S. Velghe, J. Primot, N. Guérineau, M. Cohen, and B. Wattellier, "Wave-front reconstruction from multidirectional phase derivatives generated by multilateral shearing interferometers," *Opt. Lett.* **30**, 245–247 (2005).
14. R. G. Lane and M. Tallon, "Wave-front reconstruction using a Shack-Hartmann sensor," *Appl. Opt.* **31**, 6902–6908 (1992).
15. R. Borrego-Varillas, C. Romero, J. R. V. de Aldana, J. M. Bueno, and L. Roso, "Wavefront retrieval of amplified femto-second beams by second-harmonic generation," *Opt. Express* **19**, 22851–22862 (2011).
16. G. P. Andersen, L. Dussan, F. Ghebremichael, and K. Chen, "Holographic wavefront sensor," *Opt. Eng.* **48**, 085801 (2009).
17. C. Schulze, D. Naidoo, D. Flamm, O. A. Schmidt, A. Forbes, and M. Duparré, "Wavefront reconstruction by modal decomposition," *Opt. Express* **20**, 19714–19725 (2012).
18. N. Hodgson and H. Weber, *Laser Resonators and Beam Propagation* (Springer, 2005).
19. T. Kaiser, D. Flamm, S. Schröter, and M. Duparré, "Complete modal decomposition for optical fibers using CGH-based correlation filters," *Opt. Express* **17**, 9347–9356 (2009).
20. ISO, "Lasers and laser-related equipment—Test methods for determination of the shape of a laser beam wavefront—Part 1: Terminology and fundamental aspects," ISO 15367-1:2003, 2003.
21. C. Schulze, S. Ngcobo, M. Duparré, and A. Forbes, "Modal decomposition without a priori scale information," *Opt. Express* **20**, 27866–27873 (2012).
22. D. Flamm, D. Naidoo, C. Schulze, A. Forbes, and M. Duparré, "Mode analysis with a spatial light modulator as a correlation filter," *Opt. Lett.* **37**, 2478–2480 (2012).
23. V. Arrizón, U. Ruiz, R. Carrada, and L. A. González, "Pixelated phase computer holograms for the accurate encoding of scalar complex fields," *J. Opt. Soc. Am. A* **24**, 3500–3507 (2007).
24. W.-H. Lee, "Binary computer-generated holograms," *Appl. Opt.* **18**, 3661–3669 (1979).
25. M. Born and E. Wolf, *Principles of Optics*, 7th ed. (Cambridge University, 1991).
26. J. L. Rodgers and W. A. Nicwander, "Thirteen ways to look at the correlation coefficient," *Am. Statist.* **42**, 59–66 (1988).